



CHORUS

This is the accepted manuscript made available via CHORUS. The article has been published as:

Buckling Causes Nonlinear Dynamics of Filamentous Viruses Driven through Nanopores

Angus McMullen, Hendrick W. de Haan, Jay X. Tang, and Derek Stein

Phys. Rev. Lett. **120**, 078101 — Published 12 February 2018

DOI: [10.1103/PhysRevLett.120.078101](https://doi.org/10.1103/PhysRevLett.120.078101)

Buckling Causes Nonlinear Dynamics of Filamentous Viruses Driven through Nanopores

Angus McMullen,¹ Hendrick W. de Haan,² Jay X. Tang,¹ and Derek Stein¹

¹*Physics Department, Brown University, Providence, Rhode Island 02912, USA*

²*Faculty of Science, University of Ontario Institute of Technology, Oshawa, ON, L1H-7K4, Canada*

Measurements and Langevin dynamics simulations of filamentous viruses driven through solid-state nanopores reveal a superlinear rise in the translocation velocity with driving force. The mobility also scales with the length of the virus in a nontrivial way that depends on the force. These dynamics are consequences of the buckling of the leading portion of a virus as it emerges from the nanopore and is put under compressive stress by the viscous forces it encounters. The leading tip of a buckled virus stalls and this reduces the total viscous drag force. We present a scaling theory which connects the solid mechanics to the nonlinear dynamics of polyelectrolytes translocating nanopores.

The buckling of a column under compression occurs in systems that span an enormous range of scales, from rail tracks and pipelines [1, 2] down to the microtubules in a living cell [3–5]. The mechanical buckling instability, first elucidated by Euler, arises from a competition between elasticity and compressive stress [6]. Elasticity tends to restore a bent rod to its linear, equilibrium conformation, whereas a compressive stress applied along the rod’s axis exacerbates departures from linearity. An instability sets in when the compressive stress grows too large or the rod grows too long for the rod’s elasticity to counteract the growth of deformations, and the rod buckles sideways. Here, we report measurements and Langevin dynamics (LD) simulations that reveal the buckling of filamentous viruses as they translocate a voltage-biased nanopore due to the viscous drag forces that compress the leading part of the polymer as it emerges from the nanopore. Buckling profoundly affects the translocation dynamics, giving rise to a nonlinear electrophoretic mobility and a nontrivial dependence on the virus length. A scaling theory captures these new dynamical effects.

A nanopore is a nanometer-scale hole in a thin membrane that can detect translocations by large polyelectrolytes like DNA or filamentous viruses. Nanopore technology is being developed for bioanalysis applications, notably DNA sequencing [7]. A voltage ΔV applied between fluid reservoirs on either side of a nanopore drives the polyelectrolyte from the *cis* side to the *trans* side, as illustrated in Fig. 1. The voltage also drives an ionic current I whose disruption signals the polymer’s presence inside the nanopore [8, 9]. The force driving the polymer is exerted mainly on the part inside the nanopore [10, 11], and that localized force is balanced by viscous drag forces that are distributed unevenly over the entire polymer. The forces generate tension in the part of the polymer on the *cis* side and compression on the *trans* side. For long DNA molecules, the tension and its propagation through the coil on the *cis* side give the mean translocation velocity a nontrivial length-dependence [12–18] and cause large velocity fluctuations [19–21]. The behavior of the *trans* portion of the polymer has so far been neglected; it

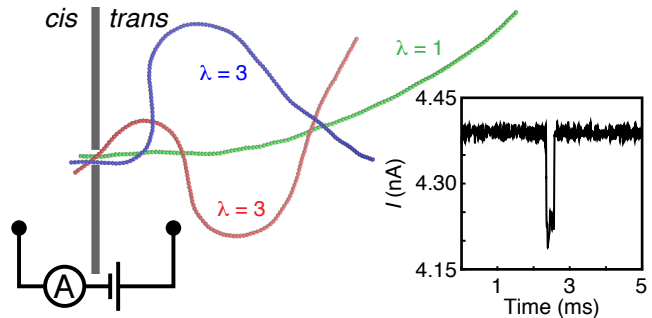


FIG. 1. Simulated virus configurations near the end of nanopore translocations with $\lambda=1$ (green polymer) and $\lambda=3$ (buckled red and blue polymers). Inset: I trace measured during an *fd* translocation of a 29 nm diameter nanopore.

is generally assumed that the part that has translocated has little effect.

Our studies of the filamentous viruses *fd* and Y21M challenge that view. The high stiffness of those viruses compels most of their length to move at the translocation speed, which generates large viscous drag forces outside the nanopore. We have discovered a direct connection between the occurrence of buckled configurations of the polymer on the *trans* side and nonlinear dynamical behavior. Previously, only a linear dependence of the mean translocation speed v on ΔV has been measured [22–25] or predicted theoretically [26, 27].

We measured virus translocations through solid-state nanopores as described in Ref. [24]. Briefly, a nanopore drilled through a 20 nm-thin silicon nitride membrane on a silicon chip connected two reservoirs containing aqueous 200 mM KCl, 10 mM Tris, 1 mM EDTA solution at pH 8. We applied ΔV and measured I using a current amplifier attached to Ag/AgCl electrodes immersed in the reservoirs. I was low pass filtered at 50 kHz, which gave sufficient bandwidth to resolve the shortest translocation durations relevant to this study. Filamentous viruses were grown using X11-Blue as the host *E. coli* strain [28]. The purified *fd* viruses, whose length is $L=0.88 \mu\text{m}$ and persistence length is $P = 2.8 \mu\text{m}$, also in-

clude small percentages of dimers and trimers, which are 2 and 3 times the length of *fd*, respectively. Those dimers and trimers enabled us to study the length dependence of the virus translocations. We also studied Y21M, a mutant of *fd* with the same length and charge density but a longer persistence length, $P = 9.9 \mu\text{m}$. The viruses, which are negatively charged, were electrophoretically drawn through the nanopore, causing transient blockages in I , an example of which appears in Fig. 1. We determined the duration τ and the amplitude $\langle \Delta I \rangle$ of each blockage from a least-squares fit of a square pulse. We obtained the mean translocation speed v by fitting a first passage time function to distributions of τ (see Supplemental Material, which contains Refs. [29–32]). We discarded signals caused by side-on collisions of the virus with the nanopore, which were easily identified by their low $\langle \Delta I \rangle$ and short τ [24].

We also performed LD simulations that enable us to visualize polymer configurations, instead of merely inferring them from the translocation dynamics. A polymer was comprised of N monomers linked by a finitely extensible nonlinear elastic potential [33, 34]. The excluded volume was given by the Weeks-Chandler-Anderson potential [35] and the polymer stiffness imposed by a harmonic bending potential tuned to match the stiffness of *fd*. A polymer with $N=133$ has the same aspect ratio as *fd*. Lu *et al.* calculated that the electrokinetic force on a monomer depends on its radial position r inside a cylindrical nanopore [36]; as a polyelectrolyte approaches the nanopore wall, the changes in the electroosmotic flow profile increase the driving force [36]. We used the theoretically predicted force profile, $F(r)$ (see Supplemental Material), and localized it inside the nanopore (i.e. it was zero outside). We multiplied $F(r)$ by a scaling factor λ to adjust the magnitude of the force. We can convert λ into experimental ΔV values by matching the Peclet numbers of simulated and measured polymers (see refs. [24, 37]).

Figure 2(a) shows the dependence of v on ΔV for *fd* translocations of a 19 nm diameter nanopore and for both *fd* and Y21M translocations of a 22 nm diameter nanopore. *fd* translocations were measured with ΔV as high as 400 mV in an effort to probe the limits of the linear mobility regime; it was important to work with very dilute *fd* suspensions in order to avoid the nanopore clogging at the highest voltages. v grew superlinearly with ΔV in all cases. The dependence was slightly more superlinear for *fd* than for the stiffer Y21M mutant, which indicates a role for the viruses' mechanical properties in shaping the translocation dynamics. The inset of Fig. 2 plots the dependence of v on ΔV for translocations of a 29 nm diameter nanopore by *fd*, *fd* dimers, and *fd* trimers. The dimers and trimers appear to depart from linearity at lower voltages than the monomers, but the measurements show too much uncertainty to establish a length dependence. The mobility of *fd* varied modestly between the three nanopores, which could be explained by the

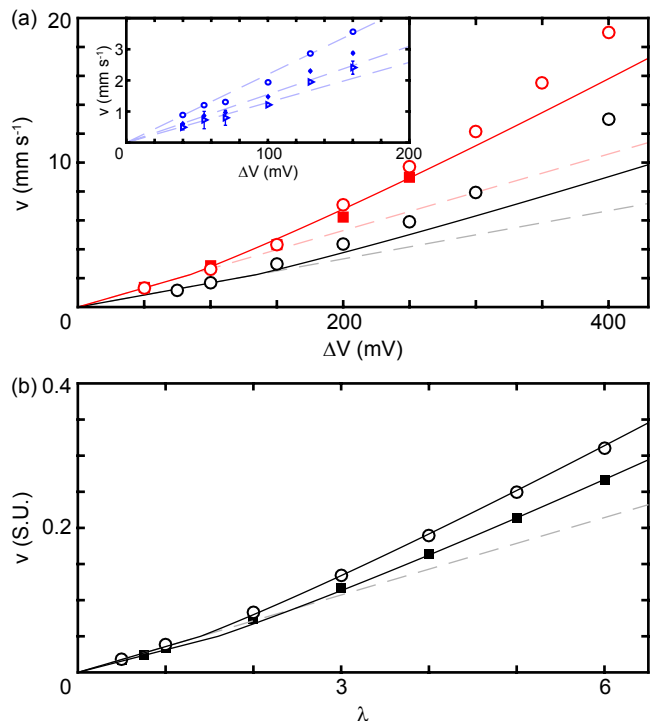


FIG. 2. (a) v vs. ΔV for translocations of nanopores with diameters of 19 nm (black) and 22 nm (red) by *fd* virus (circles) and the stiffer Y21M mutant (squares). Inset: v vs. ΔV for *fd* (circles), *fd* dimers (diamonds), and *fd* trimers (triangles) in a 29 nm diameter nanopore. (b) v vs. λ for simulated translocations by filaments of stiffness comparable to *fd* (circles) and Y21M (squares). Solid lines represent the scaling theory presented in the main text. Dashed lines show extrapolations of the linear mobility regime.

diameter-dependence of the electrokinetic driving force and drag coefficient [11], and possibly also by differences in the surface charge of the nanopores [24].

The simulated polymers exhibited a similar superlinear rise in v with λ , seen in Fig. 2(b), which was more pronounced for a polymer whose stiffness matched that of *fd* than for a polymer matching Y21M.

Figure 3 shows the decreasing average mobility of *fd*, $v\Delta V^{-1}$, with L for translocations of a 29 nm diameter nanopore for four different values of ΔV . The L -dependence grew weaker as ΔV increased. Simulations similarly found that the average mobility decreased with N at a rate that decreased with increasing λ (Fig. 3).

Figure 4(a) plots the evolution of the instantaneous mobility (whose calculation is detailed in the Supplemental Material) of a simulated polymer over the course of translocations for various N and λ . The data are normalized by the mobility of a rigid rod in bulk solution in order to factor out the trivial N -dependence expected from the Stokes drag. The mobility equals the bulk mobility in the early part of translocations, then rises toward the end, with the rise beginning earlier and bending more sharply as λ increases. The mobility also rises earlier and

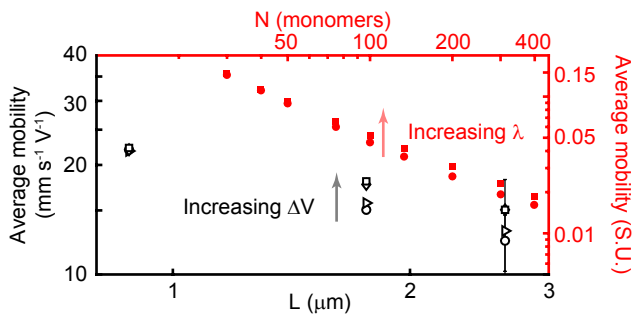


FIG. 3. L -dependence of the average mobility in translocations of a 29 nm diameter nanopore by fd with $\Delta V=40, 55, 130,$ and 160 mV (black). Also plotted is the N -dependence of the average mobility of simulated polymers (red) for $\lambda = 0.5$ and 2 . Error bars are standard deviations found by bootstrap resampling of the data.

more sharply as N increases.

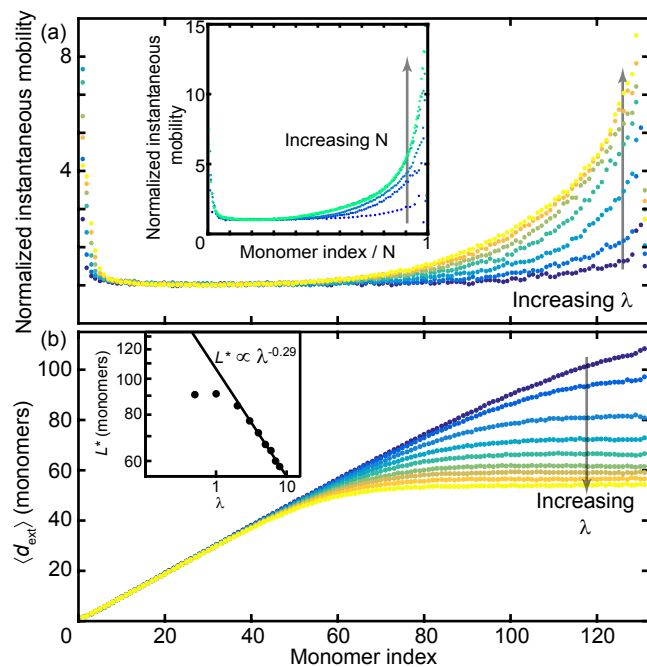


FIG. 4. (a) Evolution of the instantaneous filament mobility during translocations by simulated polymers for various λ . The inset plots the same dependence for $N = 50, 100, 133, 200,$ and 266 with $\lambda = 1$. (b) Evolution of $\langle d_{\text{ext}} \rangle$ over the course of simulated translocations for various λ . The inset shows the dependence of L^* on λ ; the line is a power-law fit to the high- λ behavior. (a) and (b) show $\lambda = 0.5, 1, 2, 3, 4, 5, 6, 7$ and 8 , ordered as indicated.

The simulations provide clear evidence of buckling and its connection to the nonlinear rise in v with ΔV . Figure 4(b) shows the evolution of the mean distance between the nanopore and the leading monomer of the virus $\langle d_{\text{ext}} \rangle$ as a function of the number of monomers that have translocated the nanopore. The leading monomer initially moves steadily away from the nanopore, with

$\langle d_{\text{ext}} \rangle$ equal to the length of polymer that has translocated. Eventually $\langle d_{\text{ext}} \rangle$ stalls, even as more monomers pass through the nanopore. The stall signals the buckling of the polymer. Figure 1 shows two typical buckled configurations at $\lambda = 3$. Note that the onset of buckling in Fig. 4(b) coincides with the onset of the acceleration observed in Fig. 4(a). The influence of buckling on mobility was also observed *within* ensembles of translocation events, as a polymer's translocation time increased with its end-to-end extension after the translocation for fixed λ (see Supplementary Fig. 3). Buckling leads to an acceleration of the translocation because each monomer that stalls (or slows) experiences no (or less) viscous force, so the driving force faces less resistance. We also observed that buckled polymers consistently become pinned, either against one side of the nanopore (e.g. Fig. 1, blue polymer) or against both in a cross-pore configuration (e.g. Fig. 1, red polymer), which further accelerates the translocation because $F(r)$ is highest at the perimeter of the nanopore. Because our simulation includes no polymer-pore interaction beyond excluded volume, the pinning is a purely mechanical effect. The critical distance at which buckling occurs decreases with λ with a power law dependence $L^* \propto \lambda^{-0.29}$ (inset of Fig. 4(b)). For the lowest λ 's investigated, the polymer did not buckle catastrophically. Our determination of L^* for $\lambda \leq 2$ were inaccurate because of this absence of strong buckling. To illustrate these observations, Supplementary Videos show an $N = 133$ long polymer buckling with $\lambda = 6$ but not $\lambda = 1$, and a shorter $N = 50$ polymer avoiding buckling at both $\lambda = 6$ and $\lambda = 1$.

As a virus emerges from a nanopore, each segment on the *trans* side must push the entire length of polymer in front of it. The Stokes drag on a slender rod of length L and radius a being pushed from behind to a velocity v through a fluid of viscosity η is

$$F_v(L) = \frac{2\pi\eta L}{\log(L/2a)}v \quad (1)$$

(the small contribution to the total viscous drag from the part of the virus that is inside the nanopore is neglected). The compressive stress in the virus therefore increases with distance from the leading tip. This is analogous to the increasing compressive stress in a massive freestanding column with distance from the top due to gravity. Euler's formula gives the critical length L^* where the self-buckling instability sets in

$$L^* = \left(\frac{9(j_{1/3})^2 EI}{4q} \right)^{1/3}, \quad (2)$$

where E is the elastic modulus, I is the moment of inertia, q is the force per unit length, and $j_{1/3} \approx 1.86635$ is the first zero of the Bessel function of the first kind of order $1/3$ [38]. Combining eqs. 1 and 2 and using

$P = EI/k_B T$, we find $\frac{(L^*)^3}{\log(L^*/2a)} \approx \frac{1.247 P k_B T}{\eta v}$. Neglecting the logarithmic length dependence and defining a critical translocation velocity v_c beyond which the buckling transition sets in for a rod of length L , we obtain

$$\frac{L^*}{L} \approx \left(\frac{v_c}{v}\right)^{1/3}. \quad (3)$$

Now we show how the nonlinear translocation dynamics of viruses are a direct consequence of buckling. The instantaneous translocation velocity ds/dt is determined by the balance of forces $\frac{ds}{dt} = F/\xi(s)$, where F is the driving force and $\xi(s)$ is the viscous drag coefficient of the rod after a length s has translocated. The dynamics are found by integrating over the translocation

$$\int_0^L \xi(s) ds = \int_0^\tau F dt, \quad (4)$$

with τ the total translocation time. We take the viscous drag on the virus before buckling to be $\xi = \gamma L$, where γ is the drag per unit length for a stiff rod. When the virus buckles, the leading tip stalls and the average velocity of the *trans* part becomes less than $\frac{ds}{dt}$. Buckling accelerates the translocation because the buckled virus experiences less viscous drag. We estimate the average velocity of the virus between the nanopore and the leading tip to be $\alpha \frac{ds}{dt}$, with $\alpha \approx \frac{1}{2}$ because the velocity must rise continuously from 0 at the stalled tip to $\frac{ds}{dt}$ at the nanopore. This model of buckling leads to

$$\begin{aligned} \xi(s) &= \gamma L \quad (s \leq L^*); \\ &= \gamma(L-s) + \alpha \gamma s \quad (s > L^*). \end{aligned} \quad (5)$$

The driving force on a virus is F_0 before it buckles. After buckling, the virus becomes pinned to the side of the nanopore where the electrokinetic driving force becomes $F = \beta F_0$, taking for simplicity $\beta \approx 2$ from the electrokinetic model of $F(r)$. While this increase in the driving force after buckling is not needed to find nonlinear dynamics, it improves the quantitative predictions and it is consistent with what we know about the viruses' general behavior from our simulations.

To find the relationship between ΔV and v , we first integrate eq. 4, breaking the translocation into two intervals, one before buckling ($s \leq L^*$) and the other after buckling ($s > L^*$), using the appropriate expressions for F and $\xi(s)$ in each. τ is the sum of the two intervals. Next we use $v = L/\tau$ to eliminate τ , and eq. 3 to convert the remaining L -dependence into a dependence on v . Finally, we define ΔV_c to be the critical voltage for buckling to occur in a polymer of length L and use the fact that $F_0 \propto \Delta V$ to obtain

$$\Delta V = \Delta V_c \left(\frac{v}{v_c}\right) \left(A + B \left(\frac{v_c}{v}\right)^{1/3} + C \left(\frac{v_c}{v}\right)^{2/3} \right). \quad (6)$$

A , B , and C are constants that depend on whether the virus is shorter or longer than L^* . Below the buckling

threshold ($L < L^*$), $A = 1$ and $B = C = 0$. Above the buckling threshold ($L > L^*$), $A = \frac{1}{2\beta}(\alpha + 1)$, $B = 1 - \frac{1}{\beta}$ and $C = \frac{1}{2\beta}(1 - \alpha)$.

Equation 6 describes the measured data in Fig. 2 quite well. The model captures the superlinear rise in v with ΔV after an initial linear regime, as well as the slightly slower rise for the stiffer polymer. Fitting eq. 6 using v_c and ΔV_c as free parameters, the *fd* measurements give $v_c = 2.25 \text{ mm s}^{-1}$ and $\Delta V_c = 85 \text{ mV}$ (135 mV) for the 19 nm (22 nm) nanopore. The data rise more rapidly than the model at high ΔV ; this could be explained by a larger jump in the force experienced by a buckled polymer than modeled (i.e. a larger β) or by a larger reduction in the drag after buckling (i.e. a smaller α). For the simulation data, the fits are excellent, and we found $v_c = 0.05$ and $\lambda_c = 1.4$ for *fd*, and $v_c = 0.055$ and $\lambda_c = 1.7$ for Y21M.

The buckling model also explains the L - and ΔV -dependence of the mobility plotted in Fig. 3. For a given length of polymer, buckling occurs earlier in the translocation as ΔV increases, which increases the average mobility. Also, the scaling model predicts $\Delta V_c \sim 1/L$, so longer polymers experience a relatively greater reduction in drag, and their mobility grows more rapidly with ΔV . Finally, the model predicts the high- λ dependence of L^* shown in Fig. 4. Because the driving force is proportional to v up until the buckling transition, eq. 3 leads to $L^* \propto \lambda^{-1/3}$, which is very close to the scaling $L^* \propto \lambda^{-0.29}$ observed in the simulations.

Interestingly, the onset of buckling observed in translocation experiments and simulations occurred at higher forces and speeds than expected theoretically. Based on eqs. 1 and 2 and the known mechanical properties of *fd*, we estimated $v_c = 83 \text{ } \mu\text{m/s}$, which is about 27 times smaller than the value we obtained from the dynamics in Fig. 2. Similarly, we estimated $v_c = 0.0014$ for the simulated *fd* virus, which is about 35 times less than the value we obtained from the dynamical simulations. We speculate that two neglected effects would explain this discrepancy. The first is thermal fluctuations, which play a dual role of nucleating bends that can lead to buckling while also shedding stress by reducing curvature in bent sections. The second is the selection of fast buckling modes by the short translocation time; only buckling modes that are fast enough to distort the virus significantly before the translocation ends will affect the dynamics. These complicated but interesting effects should be studied in future work.

In conclusion, we discovered a connection between the solid mechanics and the dynamics of filamentous viruses translocating nanopores. The translocation velocity grows nonlinearly with the driving force because the filament's leading part buckles as it emerges from the nanopore. Nonlinear dynamics have neither been predicted nor measured previously in the flexible polymers or rigid rods. The filamentous virus dynam-

ics we observed are a distinctive feature of the regime where the polymer length is comparable with the persistence length. We therefore expect buckling to occur in nanopore measurements of DNA, and for it to have a significant influence on the translocation dynamics of molecules with a length comparable to 50 nm, which is an experimentally relevant regime [39, 40].

We thank Zvonimir Dogic, Prerna Sharma, and Andrew Balchunas and acknowledge support from NSF DMR-0820492 for virus samples. We also thank Bo Lu for sharing his finite element analysis code. This work was supported by NSF DMR-1505878 and the Brown University Institute for Molecular and Nanoscale Innovation.

-
- [1] A. D. Kerr, *Journal of Applied Mechanics* **41**, 841 (1974).
 [2] R. Hobbs, *Journal of Constructional Steel Research* **1**, 2 (1981).
 [3] S. R. Heidemann, S. Kaech, R. E. Buxbaum, and A. Matas, *The Journal of Cell Biology* **145**, 109 (1999).
 [4] N. Wang, K. Naruse, D. Stamenović, J. J. Fredberg, S. M. Mijailovich, I. M. Tolić-Nørrelykke, T. Polte, R. Mannix, and D. E. Ingber, *Proceedings of the National Academy of Sciences of the United States of America* **98**, 7765 (2001).
 [5] C. P. Brangwynne, *The Journal of Cell Biology* **173**, 733 (2006).
 [6] A. P. Boresi, R. J. Schmidt, and O. M. Sidebottom, *Advanced mechanics of materials*, Vol. 5 (Wiley New York, 1993).
 [7] D. Branton, D. W. Deamer, A. Marziali, H. Bayley, S. A. Benner, T. Butler, M. Di Ventra, S. Garaj, A. Hibbs, S. B. Jovanovich, P. S. Krstic, S. Lindsay, X. Sean, C. H. Mastrangelo, A. Meller, J. S. Oliver, Y. V. Pershin, J. M. Ramsey, R. Riehn, G. V. Soni, V. Tabard-cossa, M. Wanunu, M. Wiggin, and J. A. Schloss, *Nature Biotechnology* **26**, 1146 (2008).
 [8] J. J. Kasianowicz, E. Brandin, D. Branton, and D. W. Deamer, *Proceedings of the National Academy of Sciences of the United States of America* **93**, 13770 (1996).
 [9] J. Li, D. Stein, C. McMullan, D. Branton, M. J. Aziz, and J. A. Golovchenko, *Nature* **412**, 166 (2001).
 [10] U. F. Keyser, B. N. Koeleman, S. van Dorp, D. Krapf, R. M. M. Smeets, S. G. Lemay, N. H. Dekker, and C. Dekker, *Nature Physics* **2**, 473 (2006).
 [11] S. van Dorp, U. F. Keyser, N. H. Dekker, C. Dekker, and S. G. Lemay, *Nature Physics* **5**, 347 (2009).
 [12] T. Sakaue, *Physical Review E* **81**, 041808 (2010).
 [13] A. Y. Grosberg, S. Nechaev, M. Tamm, and O. Vasilyev, *Physical Review Letters* **96**, 228105 (2006).
 [14] I. Huopaniemi, K. F. Luo, T. Ala-Nissila, and S. C. Ying, *Physical Review E* **75**, 061912 (2007).
 [15] A. Bhattacharya, W. H. Morrison, K. Luo, T. Ala-Nissila, S. Ying, A. Milchev, and K. Binder, *The European physical journal. E, Soft matter* **29**, 423 (2009).
 [16] B. Lu, F. Albertorio, D. P. Hoogerheide, and J. A. Golovchenko, *Biophysical Journal* **101**, 70 (2011).
 [17] T. Ikonen, A. Bhattacharya, T. Ala-Nissila, and W. Sung, *Journal of Chemical Physics* **137**, 085101 (2012).
 [18] T. Saito and T. Sakaue, *Physical Review E* **88**, 042606 (2013).
 [19] A. J. Storm, C. Storm, J. Chen, H. Zandbergen, J. F. Joanny, and C. Dekker, *Nano Letters* **5**, 1193 (2005).
 [20] M. G. Gauthier and G. W. Slater, *The Journal of Chemical Physics* **128**, 205103 (2008).
 [21] K. Luo, I. Huopaniemi, T. Ala-Nissila, and S. C. Ying, *The Journal of Chemical Physics* **124**, 114704 (2006).
 [22] D. Fologea, J. Uplinger, B. Thomas, D. S. McNabb, and J. Li, *Nano letters* **5**, 1734 (2005).
 [23] J. Li and D. S. Talaga, *Journal of Physics: Condensed Matter* **22**, 454129 (2010).
 [24] A. McMullen, H. W. de Haan, J. X. Tang, and D. Stein, *Nature Communications* **5**, 4171 (2014).
 [25] J. Larkin, R. Y. Henley, M. Muthukumar, J. K. Rosenstein, and M. Wanunu, *Biophysical Journal* **106**, 696 (2014).
 [26] S. Ghosal, *Physical Review Letters* **98**, 238104 (2007).
 [27] S. Ghosal, *Physical Review E* **76**, 061916 (2007).
 [28] E. Barry, D. Beller, and Z. Dogic, *Soft Matter* **5**, 2563 (2009).
 [29] L. A. Day, C. J. Marzec, S. A. Reisberg, and A. Casadevall, *Annual Review of Biophysics and Biophysical Chemistry* **17**, 509 (1988).
 [30] K. Zimmermann, H. Hagedorn, C. C. Heuck, M. Hinrichsen, and H. Ludwig, *Journal of Biological Chemistry* **261**, 1653 (1986).
 [31] E. Schrödinger, *Physikalische Zeitschrift* **16**, 289 (1915).
 [32] M. V. Smoluchowski, *Physikalische Zeitschrift* **16**, 321 (1915).
 [33] G. Grest and K. Kremer, *Physical Review A* **33**, 3628 (1986).
 [34] G. W. Slater, C. Holm, M. V. Chubynsky, H. W. de Haan, A. Dubé, K. Grass, O. A. Hickey, C. Kingsbury, D. Sean, T. N. Shendruk, and L. Zhan, *Electrophoresis* **30**, 792 (2009).
 [35] J. Weeks, D. Chandler, and H. Anderson, *Journal of Chemical Physics* **54**, 5237 (1978).
 [36] B. Lu, D. P. Hoogerheide, Q. Zhao, and D. Yu, *Physical Review E* **86**, 011921 (2012).
 [37] H. W. de Haan, D. Sean, and G. W. Slater, *Physical Review E* **91**, 022601 (2015).
 [38] A. G. Greenhill, *Proc. Cambridge Philos. Soc.* **4**, 65 (1881).
 [39] S. Carson, J. Wilson, A. Aksimentiev, and M. Wanunu, *Biophysical Journal* **107**, 2381 (2014).
 [40] J. K. Rosenstein, M. Wanunu, C. A. Merchant, M. Drndic, and K. L. Shepard, *Nature Methods* **9**, 487 (2012).